2020

Adaptive Background Correction of Crystal Image Datasets: Towards Automated Process Control

Luke Kiernan
Innopharma Technology, Dublin

Ian Jones
Innopharma Technology, Dublin

Lauri Kurki
VTT Technical Research Center of Finland

See next page for additional authors

Recommended Citation

Kiernan, L., Jones, I., Kurki, L. et al. Adaptive Background Correction of Crystal Image Datasets: Towards Automated Process Control. Sens Imaging 21, 48 (2020). DOI: 10.1007/s11220-020-00310-6

Funder: EC's Seventh Framework; Science Foundation Ireland

Sensing and Imaging (2020) 21:48
https://doi.org/10.1007/s11220-020-00310-6

ORIGINAL PAPER

Adaptive Background Correction of Crystal Image Datasets: Towards Automated Process Control

Luke Kiernan[1] · Ian Jones[1] · Lauri Kurki[2,3] · Patrick J. Cullen[4] · Toufic El Arnaout[5,6]

Received: 21 June 2020 / Revised: 3 August 2020 / Accepted: 12 September 2020 /
Published online: 3 October 2020

Abstract

Improving the data descriptor calculation of crystal's physical properties requires sophisticated imaging techniques and algorithms. It has been possible to construct 2D population balance models benefiting from characteristic measurements of both crystal's length and width, compared to the single representative sizes used in 1D models. Our aim is to ameliorate the procedure of determining shape (and not only size) factors, in an automated fashion and directly from the process, for implementation in future models. Here, approaches suitable for real-time applications were employed including engineered imaging sensors and adaptive algorithms. We described the latter in detail for varying 2D image datasets. Their basic concept is similar. Each is applicable to an entire dataset, thus demonstrating efficacy for a variety of particle environments. While the challenge of particle segmentation for higher concentrations was not scrutinized here, this approach reduced processing time, steps and supervision, for the benefit of certain applications requiring process monitoring and automation.

Electronic supplementary material The online version of this article (https://doi.org/10.1007/s11220-020-00310-6) contains supplementary material, which is available to authorized users.

✉ Toufic El Arnaout
toufic.arnaout@kappacrystals.com

1 Innopharma Technology, Sandyford, Dublin, Ireland

2 Timegate Instruments, 90590 Oulu, Finland

3 VTT Technical Research Center of Finland, 90570 Oulu, Finland

4 School of Chemical and Biomolecular Engineering, The University of Sydney, Darlington, NSW 2008, Australia

5 School of Food Science and Environmental Health, TU Dublin - City Campus, Technological University Dublin, Dublin, Ireland

6 Kappa Crystals Ltd, Dublin, Ireland

Graphic Abstract

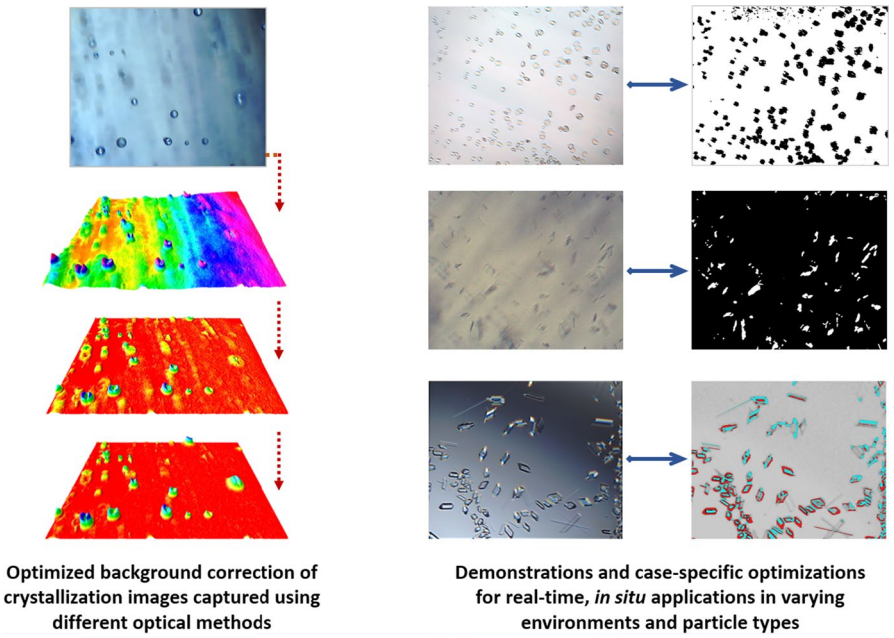

Keywords Crystallization imaging · Adaptive background correction · Particle engineering · Analytical technology

1 Introduction

1.1 Crystallization Modelling

Several spectroscopic, laser and imaging methods now permit access to information in real-time and directly from the reaction (in situ) due to developments in Process Analytical Technology (PAT) [1, 2]. This information may be crystal size distributions (CSD) and particle size-shape distribution (PSSD), and many physico-chemical properties, found to influence population balance equations (PBEs) and models (PBMs) [3]. 2D models supported by size and shape information, mainly possible using imaging, have large advantages over basic 1D models and less assumptions.

One of the main approaches employed to measure 1D information has been based on the chord length, represented by the scanned distance, in a random part across a particle. The method is highly rapid and efficient for a wide range of applications and concentrations. The CSD may be calculated based on necessary transformations from the chord length distribution (CLD). The chord length is a random scan of a particle that may result in different values for the same particle, according to its shape, rotation, physical properties, scan direction, as well as the optical properties

of the system [4] (Table 1). More recently, improved models were produced to support the calculation of 1D CSD through an optimized relationship between CLD, geometry and size [5], along with considerations of sample properties, laser intensity, refractive indices, crystal velocity, and mathematical optimizations based on the working principles of the laser beam in operation. As for the 2D CSD, additional parameters to the CLD are necessary [6], and this can be supported by using optical imaging.

Video microscopy permits not only the determination of length and width, but the shape (in 2D), including symmetry, convexity/smoothness, and circularity. Some challenges can be the performance, algorithms for image processing and understanding, sensitivity (e.g., based on resolution, refractive index, particle properties), and particle concentration. Yet, developments in microscopy have been significant and for a wide range of applications, due to an amalgamation of lenses, prisms, illumination sources, cameras, and many engineering and electronic approaches. Image and data analysis methods have also evolved [15, 16]. Therefore, imaging-based PAT has become more suitable to support monitoring, continuous crystallization and screening platforms [17, 18].

1.2 Image Processing: Developments and Challenges

An image processing workflow typically applies a series of prebuilt equations and calculations on information obtainable and accessible in the image. Several functions and plugins are available with programs like ImageJ, Rgui, Matlab and OpenCV. Certain algorithms may provide limited prediction, such as using an autocomplete function for partially complete features, sometimes with matching with a database, part of a large decision tree of sophisticated steps and loops. However, the 'interpretation' of complex images remains a challenge for machine vision as demonstrated by the inability to solve a Captcha for example, which requires human intervention.

Basic edge detection and watershed operations (e.g., Canny edge detection, Trainable Weka Segmentation (TWS)) also require significant computing times, training, use of templates [19], and/or iterative procedures. Employing a series of assumptions and line assignments (model-based) has been applied for in situ images of α-glycine crystals [20]. The technique was based on linear features, VIGs (Viewpoint-invariant groups) as properties of an object that are maintained irrespective of the camera's position, and model fitting. A method for particle recognition [21], in particular overlapped particles that are simple-shaped (e.g., rectangles) was demonstrated and used time-zero background image subtraction, multi-scale edge detection, filtering, and salient corners (intersection of two lines). More recently, the detection of simple-shaped (needles), overlapped crystals was also demonstrated for in situ applications [22]. A few studies commented on the difficulty with more complex crystal scenes including the presence of several shapes (especially not preknown), unfocused objects, high particle concentration, semi-transparent particles, and strong particle attrition. Overall, it is frequent to identify in the literature studies employing methods in parallel with microscopy, such as the CLD [14].

Table 1 A list of challenges encountered with CLD-based PAT methods

	Challenge	References
1	Detecting seeding without agitation, among other data interpretation challenges during multi-step crystallization inside a 450 L reactor	[7]
2	Challenges with transparent particles or those of similar refractive index to their surroundings. Certain dependency of the CLD on the size, shape, opacity and texture	[8, 9]
3	Variations in results, related to surface changes, and chord splitting due to sharp edges	[10]
4	Two close or overlapping particles may reflect a single chord. The effect is known as chord concatenation	[11]
5	Dependence on the particle shape (spherical vs ellipsoidal) and on the optical properties of the system (FBRM and Par-Tec 100)	[4, 12]
6	Measured CLDs of a single sized particle population: found to be very different from theoretically constructed distributions	[13]
7	Geometrical models for data interpretation: difficulty/contradiction resulted in building improved, optical models based on chord-sample relationship, laser intensity, refractive indices, crystal velocity, etc.	[5]
8	Length measurement of particles of high aspect ratio (e.g., needles)	[14]

1.3 Adaptive Background Correction

Background correction is a major task for in situ image processing for the purpose of quantitative analysis of size-shape. Most often, users subtract time-zero blank images for correction. However, typical backgrounds from in situ images are not identical throughout an entire dataset, coupled with varying noise distributions, shadows, and inhomogeneities (Figs. 1, bottom and 3). Basic median filter to subtract standard backgrounds may eliminate noise and non-homogeneity [23], but with rejection of particles smaller than 24 μm (30×30 pixels^2). Moreover, several methods of data transformation exist (e.g., linear, convolution, Gaussian, smoothing, Fourier transform). Fortunately, an adaptive approach adopted here permits normalization of such backgrounds [24] while also smoothing the image. In this paper, the technique employed is compatible with gradients, observable in certain relief contrast methods (Fig. 1, bottom) used to observe texture particularly for small and thin entities.

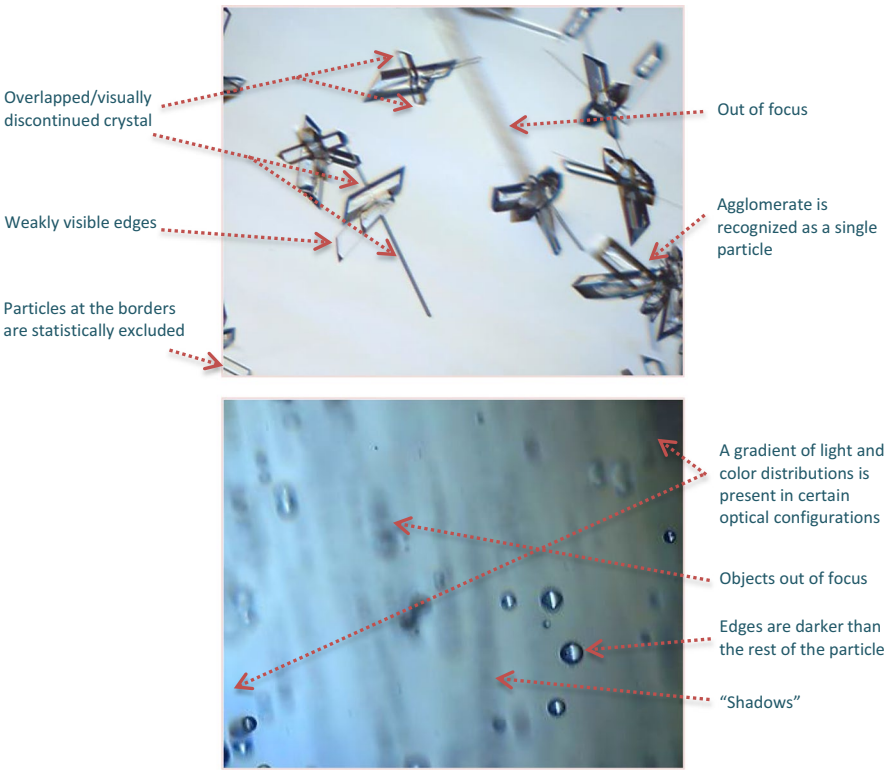

Fig. 1 Classic challenges of processing images of particles such as crystals. Top: Crystals are optically active causing difficulty compared to opaque particles. Bottom: Challenges with optical engineering setups like prism intensity and gradient. These are two examples of limitations for classic algorithms that follow a sequence of calculations, unable to resolve visually overlapped particles versus agglomerates, watershed/segmentation, out-of-focus particles, gradients of lights, and high concentrations

Visibility conditions in general impact on many measurement technologies [25]. The signal to noise and signal to background ratios (can be due to the imaging approach and/or the camera sensor [26]), illumination, gradients, and color variations, are important to optimize. Furthermore, in situ imaging challenges (Table 2) are a focus of the macro algorithms developed here.

The Rolling Ball (RB) algorithm [24] is an adaptive method for background correction, independently of time-zero/blank images or of one image to another. With the optimized sliding paraboloid (SP) approach it has been applied in the biomedical, cell biology, geophysical, and materials science sectors [31–33]. It is sufficiently fast for real-time analysis and suitable for non-uniform backgrounds (e.g., illumination, intensity, brightness, gradient). The code was successfully implemented initially in the NIH Image Pascal, which has since been superseded by ImageJ. The term "ball" describes the correcting shape that passes ('rolls') over the bottom surface of the image. It has a certain limit in reaching inside the peaks, depending on the sizes of the correction ball and the peaks. Nearly a decade ago, Michael Schmid released a variant of this algorithm, more suitable for certain images in terms of intensities and shapes, known as the "Sliding Paraboloid" of approximation (same curvature at the apex as the ball of a given radius) (Fig. 2). To be more precise, this is sometimes described as "Sliding Parabolae" in four directions (x, y and $2\times45°$), for practicality and speed reasons. The code was also optimized to correctly process objects in image corners. The parabola (or paraboloid) has a different symmetry and shape than a circle (or ball), hence the term 'sliding' rather than 'rolling' when applied. Smoothing and correction are calculated via approximate values also depending on the surrounding local average, using a pre-specified radius. A "Separate colors" option permits for RGB images to correct not only based on brightness but also on hue and saturation, which are strong visual appearance properties [34]. This possibility was key in the success of certain studies shown later, when color information was necessary from the start (Fig. 2), for in situ images containing spatial variations, blurriness, out of focus and in focus objects, shadows, and noise. It was also useful when applying an Enhanced local contrast (CLAHE) or a general 'Enhance contrast' function, via adjustments of their settings such as Blocksize, Histogram pins, Maximum slope, Mask, Histogram equalization, and Saturation.

In this study, we have listed the macros of algorithms in detail and for the respective datasets. Furthermore, the development was also explained step by step, and for several challenging experiments using explanatory figures. The study shows the main advantage of the adaptive background correction procedure employed here and the potential application opportunities to monitor processes containing particles such as cells, emulsions, bubbles, crystals, and particles in general.

2 Methods

2.1 Imaging

The imaging experiment of thiamine hydrochloride shown in Figs. 3 and 4 was carried out based on a benchtop optical system [27] under weak polarization, with a

Table 2 Possible challenges for image analysis for in situ crystallization monitoring

	Description	Solvable*	Common*
Edge versus inner contrast	Edges of imaged crystals may appear not well-defined. Edge transparency is a challenge for algorithms to correctly build the boundary	++	+
In versus out of focus	Crystal's size, shape, rotation and concentration affect its position relative to the sensor's main focal plane (e.g., 5–15 µm). Parts out of focus appear faint, blurry and incomplete	++	+++
Transparency	Very transparent/thin particles are difficult to detect, as with backward light scattering method [8]. Methods like PlasDIC may help [27]	++	+++
Shape versus completeness	Certain particle shapes and sizes, based on their rotation/projection, provide higher detected completeness. For instance, a needle has a low probability to have a chord length scan entirely along its long dimension	+	+++
3D versus 2D	2D does not provide the same information as 3D profiling due to viewing angle and rotation [28, 29]	++	++++
Particle completeness	The probability of a large particle of being fully imaged during motion inside a certain area (e.g., 1.5×1 mm^2) without touching the image borders is smaller than that of a small particle	++	+++
Particle concentration	Concentration influences background noise, variations, light recovery, crystals in focus, overlap, edge contrast, and algorithmic segmentation	+	+++
Speed in real time	Processing speed depends on the number and type of required steps, size/format and resolution of the image, frequency, and equipment performance	++++	+++
Color information	Light interaction with optically active material alters the detected light and color information, also based on the illumination and optics used including prisms	++	+++
Touching particles	Advanced watershed and segmentation algorithms may solve the challenge with touching particles to a certain extent. Complicated and random shapes make this task difficult	+	+++
Overlapping particles	Similarly to touching particles, it is not possible to extract missing information except through prediction. Many classification possibilities may exist [30] (e.g., agglomerates, overlapped, shape polymorphs)	+	+++
Microparticle versus noise	Signal to noise ratio may depend on imaging and experimental conditions. Certain threshold has to be applied while taking into consideration micro/fine particles (e.g., less than 10 µm)	+++	++
Probe design	Camera, design, dimensions, optics, sampling gap, mechatronic compatibility with the experiment as well as industrial safety and certifications, are all important to optimize in parallel with imaging quality	+++	++++
Light gradient	Gradients can be temporal, caused by solution dynamics or moving particles at different focal levels. Also due to particle concentration, and optical and illumination engineering	+++	+

Table 2 (continued)

	Description	Solvable*	Common*
Resolution versus requirement	Extra details may slow down or cause errors for algorithms: pixels of features inside large crystals may be recognized as independent particles, depending on resolution, filters, code instructions, and particle properties	++	+++
Refractive index	Crystals, solvent, density, concentration, etc., may influence on the signal in certain optical configurations	++	+++
Light distribution	Light can be unequally distributed within a particle, due to internal reflections, other neighboring particles, the concentration, and illumination	++	++
Background contribution	Crystals out of focus or at high concentrations contribute to the background noise. This should be corrected while minimally interfering with the signal of particles of interest	++	+++
Sampling	Certain spots inside a reactor may not be perfectly representative of the entire crystal size-shape population, also depending on the stirring speed, probe position, and particle properties	++	++++

*Index low (+) to high (++++) if the challenge is common with other particle characterization method, or the likeliness that it may be solved in the future

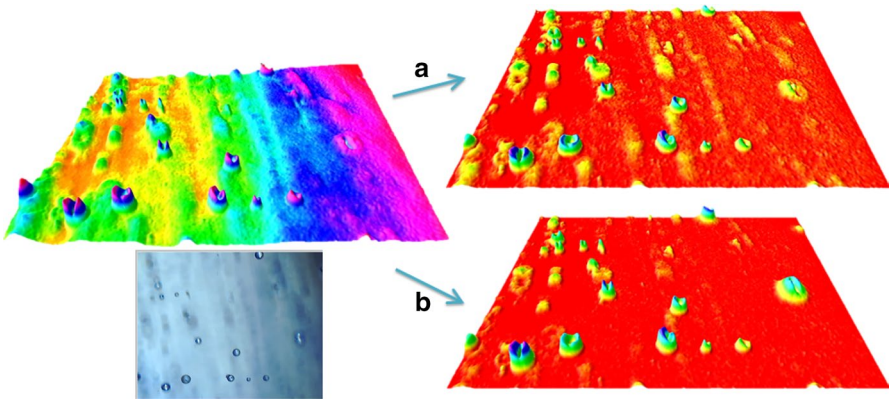

Fig. 2 The importance of continuously improving adaptive background correction algorithms. A method comparison is shown based on 3D surface plots (original raw image: bottom left) between the rolling ball (**a**) and sliding paraboloid (**b**) correction functions

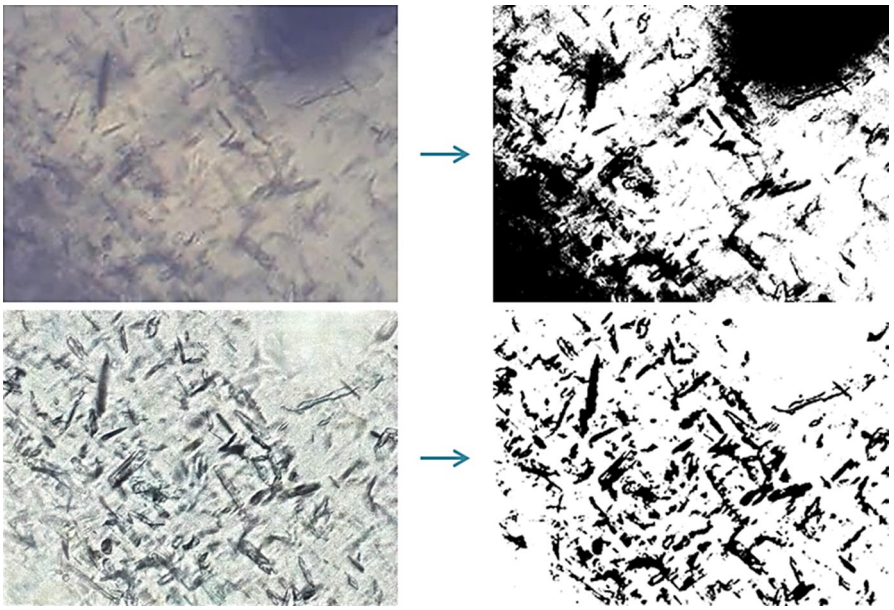

Fig. 3 A simple procedure for enhancing in-line image processing of particles. Comparison of a classic approach (raw image, top left) with an optimized one (treated image, bottom left). The resulting binary images are shown to the right

camera resolution of 2592×1944 pixels^2 and a field of view of 1.25 mm $\times$ 1 mm. Crystals were imaged as semi-opaque in low light bright field. Other experiments were imaged in bright field, moderate or strong relief contrast, on a slide (in-line) or in situ, as indicated, based on the sensor probe systems developed [27, 35] with

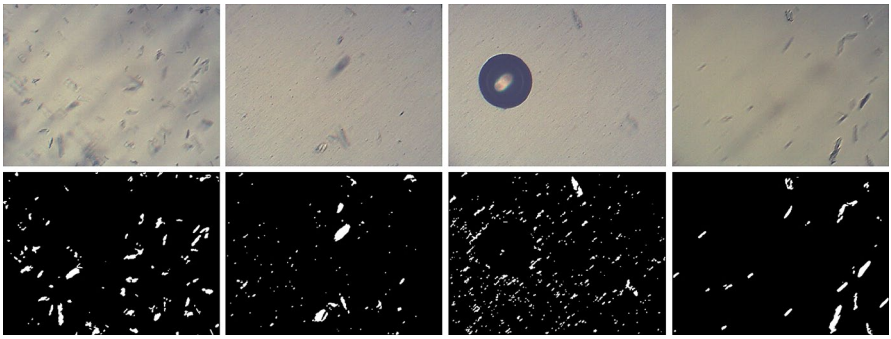

Fig. 4 A semi-adaptive approach for in-line particle image datasets. Examples are chosen from a single run whereby a single macro was applied to correct backgrounds, noise, large variations (bubbles, shadows), while preserving the signals of microparticles

a 10X objective and a camera sensor of 3376×2704 pixels^2. More specifically: (Sect. 3.1) thiamine hydrochloride crystals were imaged in a microfluidic slide with a pump system; (Sect. 3.2) lysozyme crystals were imaged statically in a large drop on a slide in bright field mode; (Sect. 3.3) particle size standards, L-glutamic acid crystals, and taurine crystals were imaged in situ with full probe immersion in relief contrast mode; finally (Sect. 3.4) taurine crystals were imaged in a large drop on a slide in relief contrast mode.

2.2 Crystallization Protocols

Thiamine hydrochloride crystals were used from a stored slurry with solvent, produced by re-crystallization.

Lysozyme was selected for the transparent crystal imaging studies with bright field mode. Lysozyme powder was first dissolved at 50 mg/mL in 0.1 M sodium acetate pH 4.5. 1 µL was then added onto a glass slide with 1 µL of precipitant (30% w/v MPEG 5000, 1 M sodium chloride and 50 mM sodium acetate pH 4.5). Additional microliters may also be used for different protein:precipitant ratios (e.g., 1:2, 1:3, 2:1). Evaporation started as the drop was visualized and crystals began forming while recording an image every 4 s.

To obtain the images shown in Fig. 7, particle standards of 15–150 µm glass beads (Malvern, Cat. QAS3002) were added to H_2O at 1% w/v and imaged during stirring. As for L-glutamic acid crystallization, it was carried out by dissolving powder at 3.5% w/v into H_2O at 65 °C, with a temperature decrease to 47 °C at a rate of 0.14 °C/min. For taurine crystallization, 100 g was added into 700 mL H_2O at 42 °C, and crystallization from supersaturation occurred over 2 h.

The last example, based on in-line imaging with a strong gradient, was carried out by adding taurine powder to 10 mL of H_2O at 95 °C until supersaturation was reached. A drop of a few µL was pipetted from the supernatant onto a microscope slide. Crystallogenesis began immediately due to evaporation and temperature decrease.

2.3 Software

Images were automatically captured using certain settings and procedures [16, 27, 35] during long experiments, or manually saved. For processing, ImageJ Fiji [36] was used for batch processing and applying the series of functions described under "Macros" below and in full detail in the Online Appendix section. For the background removal in ImageJ through the rolling ball/sliding paraboloid function, the "Separate color" function is a visible option in older versions (e.g., v. 2014 Jun 02 or v. 2014 Nov 25) possibly compared to the more recent versions some of which were heavily transitioned to Java (e.g., v. 2017 May 30 or v. 2015 Dec 22). After binary conversion and export of the particle size-shape data, Microsoft Excel was used for binning and graph generation (Fig. 6).

2.4 Macros

The image background processing and particle analysis functions applied in each experiment are shown in the Online Appendix part, Section (a). These macros (A to D) describe the procedure for each case based on the optical setting used with the crystal images they were applied on: (A) thiamine hydrochloride (Figs. 3, 4), (B) lysozyme (Fig. 5), (C) polydisperse particles, L-glutamic acid, and taurine (Fig. 7), and (D) taurine (Fig. 9).

3 Results and Discussion

3.1 In-Line Bright Field Imaging of Semi-opaque Particles

Thiamine hydrochloride crystals were observed at moderate concentrations in a low-light setting. The particles are semi-opaque in this opto-illumination setup (Fig. 1), with a strong image noise (Fig. A.1). The general strategy succeeded by following the sequence: an adaptive background subtraction (rolling ball, light background, color separation), a CLAHE contrast algorithm, smoothing, Gaussian blur smoothing, contrast enhancement, 8 bit conversion, specified thresholding (according to the brightness/contrast levels, and pixel intensities), and general binary/outlier removal/filling holes tasks. This was found to be more adequate for particle extraction and analysis compared to applying a threshold directly (Fig. 3 and Fig. A.2), to overcome the image to image variations in noise, shadows, intensities, and the presence of microcrystals or large obstructions (e.g., bubbles) (Fig. 4).

3.2 In-Line Bright Field Imaging of Transparent Crystals

Crystals are optically active due to their inherent properties and the illumination and optical imaging setup. They may appear transparent with their inner parts displaying similar intensities and color to those of the background (Fig. 5b) during

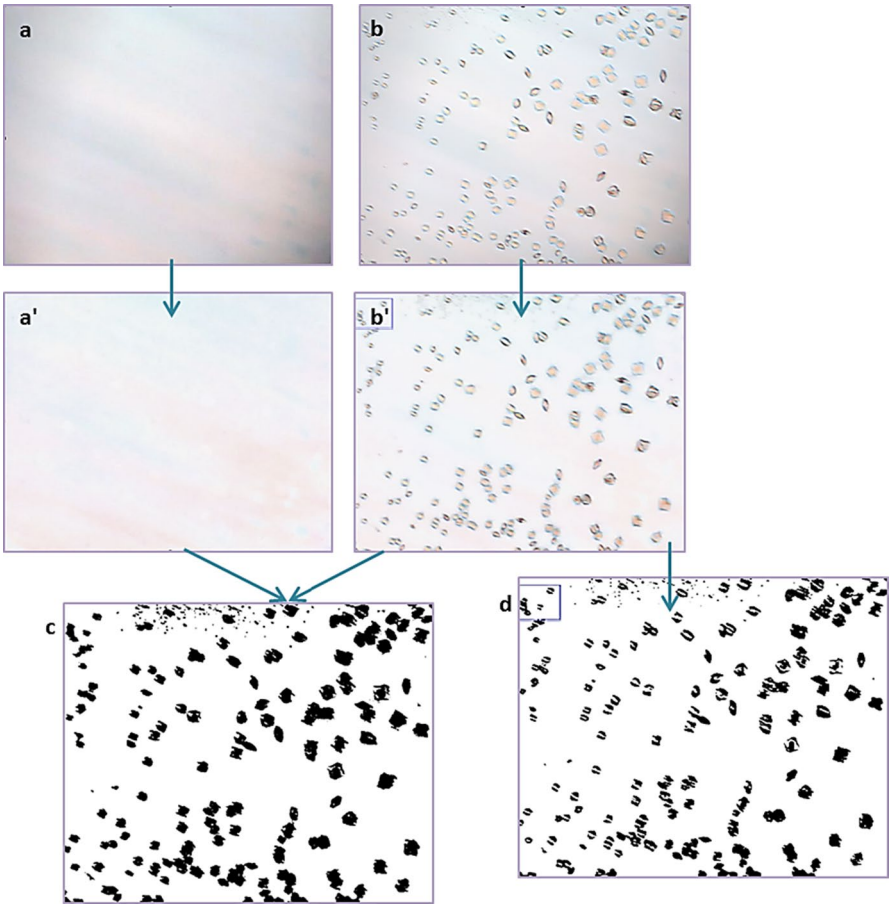

Fig. 5 Double background correction of static images of transparent crystals. Lysozyme crystals were grown by vapor diffusion. **a** The background at time zero (blank image), **a′**: the image in 'a' following correction with the rolling ball filter, **b** the crystal image (raw), **b′** the image in '**b**' after correction with the rolling ball filter, **c** thresholded and binary image of the **a′** and **b′** "Difference" calculation, **d** the non-optimized final result if the second background correction operation (with the time-zero background) was not performed

growth, as observed with benzoic acid [27]. For binary signal recovery in situations like these, a double background correction approach was found to be useful for transparent lysozyme crystals (Fig. 5c) by employing the adaptive rolling ball correction, but also a time-zero (blank image) background subtraction. This was compared against the situation whereby this double subtraction approach was not incorporated (Fig. 5). Therefore, the general procedure was to carry out a rolling ball correction of the image of interest (image 1), then, using the time-zero blank image (also rolling ball pre-corrected) (image 0), both images (0 and 1) were subtracted from each other using a 'difference create' calculation. The resulting image is then converted into 32-bit format, thresholded with specific parameters

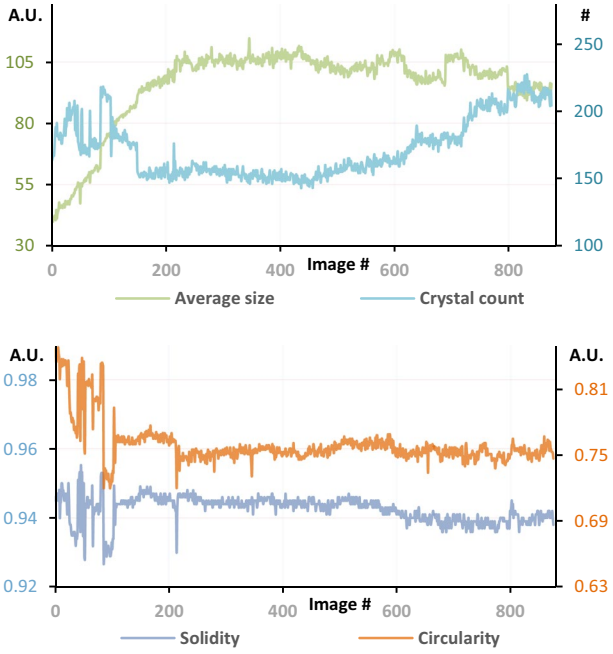

Fig. 6 Size-shape tracking of lysozyme crystals by image analysis. Average per image for all particles is shown over 800 + images. Top: average size (feret) (1 A.U. = 0.38 µm) and total counts per image. Bottom: average circularity and solidity (shape descriptors) per image as a factor (min = 0 max = 1)

and transformed into binary, before applying the usual steps of outlier correction, filling holes, smoothing, and basic watershed.

This processing approach was useful for tracking size-shape changes over 800 images (Fig. 6). During the initial stages (first 150 images), crystals grew rapidly while their positions were slowly changing (movement) before reasonably settling in the fixed optical field of view. Here, the particle analysis procedure excludes particles touching the image borders. Larger crystals were changing slightly in positions during imaging and subsequently became wholly captured within the image borders. Microcrystals decreased in counts, therefore influencing on the overall size average (jump of 3–4 µm) and counts (drop of 14%) (Fig. 6, top). Furthermore, due to the resolution requirement and optical parameters in this experiment, operating at a narrow focal plane range of < 20 µm causes certain particles to be out-of-focus. and thus strong vibrations or changes of the focal plane within the static drop may alter the processing outcome for the image recorded at that time (e.g., small peaks in images 214 and 345). Overall, rapid changes in the observed physical characteristics were most significant during the first 100 images (Fig. 6, bottom), with circularity decreasing, and shapes becoming more defined. The average size also increased until frame #215, with the total count increasing gradually after frame #460 with some influence on the size average. Therefore, this image processing has advantages to track the size at a micrometer

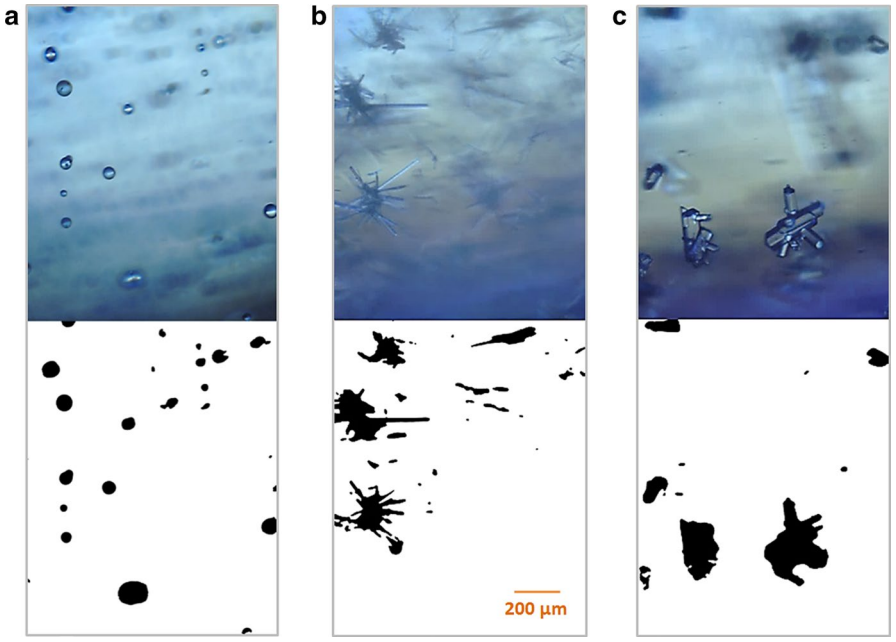

Fig. 7 Imaging particles in situ using a video microscopy probe equipped with a relief contrast imaging mode. The gradient is caused by the prism properties which are beneficial in certain applications to visualize a stronger contrast/3D-like appearance particularly for imaging small or thin features. **a** Particle size standards (15–150 µm), **b** L-Glutamic acid crystals, **c** taurine crystals. Both raw (top) and processed (bottom, binary) images are presented (rotated here 90°)

resolution, and not only shape. Nevertheless, general challenges of the imaging and processing approach employed in this paper are listed in Table 2.

3.3 In Situ Relief Contrast Imaging with a Gradient

A stronger detection of particle characteristics is desired in advanced applications aiming at texture studies or for the enhancement of weakly visible features. This may be possible via relief contrast methods including the classic DIC or more recent ones such as PlasDIC (Polarization optical differential interference contrast, or Plastic DIC) [37]. In the latter, components in the optical assembly may be reduced compared to those in DIC, while providing improved imaging flexibility and a certain compatibility with anisotropic materials [38]. However, illumination recovery is not as strong as in the bright field mode. In low noise images the user may be able to detect the natural difference between (or within) the object, and its environment in terms of the refractive index. In DIC/PlasDIC, the optical settings, including those of the main prism (and its lateral translation), may result in a gradient in the captured image (Figs. 2 and 7). In our setup, this was significant when a strong contrast was required to enhance the observation of thin/transparent particles (Fig. 9) (via illumination and/or prism adjustments). Equally the gradient effect was especially

significant during in situ imaging mode (Fig. 7). Color information also appeared to be affected and contained signals that are important to recover successfully.

To correct the background in this case, the sliding paraboloid (based on the rolling ball) method was employed. In particular, it has permitted another "color separation" option (refer to Sect. 1.3 for definition). For this application and assuming that the background is 'light' (bright mode) this approach was sufficient to process the images. The macro of the in situ image processing first and foremost started with a general, classic contrast enhancement based on a specified saturation level, with histogram equalization [39]. Combined with the relief contrast imaging approach, this proves the importance of appropriate contrast levels. Next, the background was subtracted using the sliding paraboloid method (as in Fig. 2b), in light mode, with the color separation option. The image was then converted to binary, after which general operations were applied such as outlier removal, dilation and filling holes. This procedure permitted to obtain a balance between signal recovery and noise reduction. Yet, it was more favorable with the colored, contrast enhanced images (although these take longer to process than greyscale images), than with images converted to 32 bit greyscale. Therefore, raw RGB images were necessary, to maintain the information associated with object completeness contained in color channels.

The images obtained in relief contrast mode contained a gradient (Figs. 7 and 9). In one side the taint was dark, which made the noise streaks more prominent, particularly at increasing crystal concentrations. This led to difficulties in extracting complete information. Nevertheless, examples shown here demonstrated that it is possible to extract signals into binary (Fig. 7), while the shape information is maintained. This supports the shape tracking in many applications, such as downstream processing optimization. However, the concentration challenge not only impacts on imaging (Table 2), but often on equipment, leading in some cases to the formation of a crust on the body of the probe. Yet, this happened more at the surface of the solution than inside the imaging gap, and during strong decrease from high temperatures (Fig. 8).

3.4 In-Line Relief Contrast Imaging at a Strong Prism Setting

Static drops containing transparent crystals in a single plane were used. In this experiment, it is possible to increase the relief contrast intensity via adjustment of the prism's lateral translation on top of the sample. The corresponding images exhibit a strongly visible light and contrast gradient effect. In some instances, the visualization with a strong contrast may permit the early detection of shape changes and very thin and small particles.

Taurine crystals were imaged and a macro of a double step 'light + dark' signal recovery was applied for binary extraction of signals for particle analysis purposes (Online Appendix, Algorithm D). A graphical representation of these steps is shown in Fig. 9. The raw image (left) was duplicated and then each copy was processed separately (as 'light' or 'dark'). Binary information was recovered (in red, middle) for each light or dark part and both outputs were then merged into one final image (right).

Fig. 8 Visible incrustation on an immersible probe during crystallization. The experiment included gradual decrease of temperature during which there was continuous stirring in an open container and a normally occurring evaporation. A 'crust' due to the dissolved chemical formed on the stainless steel body

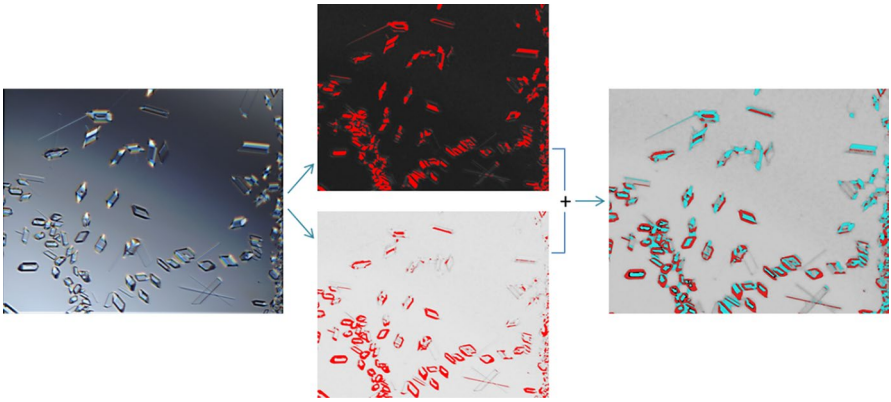

Fig. 9 Extracting transparent crystal signals from images with a strong gradient and light variation. Original image (left) is duplicated and each copy is treated separately with an adaptive background correction algorithm based on light (bright) or dark information, and then thresholded (middle). The two resulting images are then merged by adding them together (right). The cyan and red colors (right) are to show the two groups of signals recovered in the previous step (Color figure online)

In this experiment, each copy was converted to 32 bit prior to full processing. This procedure was successful for these images which contained low noise, thinner sample, and from a static drop. One copy had the background subtracted with the rolling ball, light mode, while the second copy had the correction with the rolling ball, dark mode. Thresholding for each copy was then carried out with specific threshold values (as indicated in the algorithm), optimized based on the pixel intensity thresholds, and which work for the entire dataset. Both processed copies

were then converted to binary, merged together through the "Add" operation, and saved. Particle analysis and statistics were then carried out following general operations like smoothing, filling holes, removing outliers, dilation, etc. As previously explained, in most setups, including this one, background subtraction of time-zero image was not applied, or not beneficial. It is not uncommon to rely on the blank background [21, 40], but it is not ideal in automated applications as the image backgrounds during the reaction differ from the time-zero background (particularly with in situ imaging and in the presence of an increasing particle concentration), due to light intensity changes, random particle positions, inhomogeneity and refractions, obstructions of light, etc.

4 Conclusion

An image processing workflow designated for a specific application does not randomly apply to another one. Such a workflow may also not be applicable throughout the same, entire dataset for all images. However, the background correction approach employed here was successful and time-efficient for real-time implementation (e.g., 10–30 s per image, with the possibility for multithreading images in parallel). It was possible to integrate and customize it in several procedures for different datasets. Example datasets contained varying levels of noise or distributions of pixels on different background types. These backgrounds also displayed varying gradients and intensities of brightness and colors, and with several particle transparency levels. Therefore, challenges such as noise and shadows, while maintaining the signals of microparticles were overcome. Examples presented were for (a) dark images, (b) images of transparent crystals, (c) in situ images, and (d) images of thin/transparent crystals in the presence of a strong contrast gradient.

Size-shape data descriptors were generated and their evolution between images was tracked. An additional advantage over 1D/spectroscopic/laser methods is that the reliability can be further verified by manually checking the raw images by direct observation. These descriptors do not only concern width and length (aspect ratio), as over 65% of APIs may have a median aspect ratio of 0.6–0.8 [41], but also further geometrical characteristics which are discussed including circularity and solidity (in 2D). These data descriptors will be important for the advanced modelling, change tracking, and polymorph research. Finally the work is likely to support research related to co-crystallization and/or intensified downstream processing to improve crystal characteristics with impact on efficacy, quality, safety, dissolution and bioavailability of a product [42–44].

The steps presented in this article may be also employed in the future with object classifications, decision nodes, and clustering techniques, and implemented into a large neural network [45–47], to minimize supervision and improve prediction. The major challenge to overcome remains particle segmentation. This requires advanced image understanding, recognition and continuous training. Yet, it may be case-specific when lacking the qualitative and predictive human's brain capacities necessary to solve a Captcha as a previously mentioned example.

Acknowledgements The research leading to these results has received funding from the European Community's Seventh Framework Program (FP7-SME-2013) under the CRYSTAL-VIS project, Grant Agreement Number 605814, and from Science Foundation Ireland (SFI) through a Technology Innovation Development Award (TIDA). The authors would like to thank the PAT group (TU Dublin, Ireland), VTT (Oulu, Finland), and Topchem (Ireland).

References

1. Gouveia, F. F., Rahbek, J. P., Mortensen, A. R., Pedersen, M. T., Felizardo, P. M., Bro, R., et al. (2017). Using PAT to accelerate the transition to continuous API manufacturing. *Analytical and Bioanalytical Chemistry, 409*(3), 821–832. https://doi.org/10.1007/s00216-016-9834-z.
2. Reid, L. G., Ward, W. H., Palm, A. S., & Muteki, K. (2012). Process analytical technology (PAT) in pharmaceutical development. *American Pharmaceutical Review, 15*.
3. Chen, S., Liu, T., Xu, D., Huo, Y., & Yang, Y. (2019). Image based measurement of population growth rate for L-glutamic acid crystallization. In *Chinese control conference (CCC)* (pp. 7933–7938). https://doi.org/10.23919/chicc.2019.8866441.
4. Ruf, A., Worlitschek, J., & Mazzotti, M. (2000). Modeling and experimental analysis of PSD measurements through FBRM. *Particle & Particle Systems Characterization, 17*(4), 167–179. https://doi.org/10.1002/1521-4117(200012)17:4%3c167:AID-PPSC167%3e3.0.CO;2-T.
5. Kail, N., Briesen, H., & Marquardt, W. (2008). Analysis of FBRM measurements by means of a 3D optical model. *Powder Technology, 185*(3), 211–222. https://doi.org/10.1016/j.powtec.2007.10.015.
6. Jiang, M., Zhu, X., Molaro, M. C., Rasche, M. L., Zhang, H., Chadwick, K., et al. (2014). Modification of crystal shape through deep temperature cycling. *Industrial and Engineering Chemistry Research, 53*(13), 5325–5336. https://doi.org/10.1021/ie400859d.
7. Adlington, N. K., Black, S. N., & Adshead, D. L. (2013). How to use the lasentec FBRM probe on manufacturing scale. *Organic Process Research & Development, 17*(3), 557–567. https://doi.org/10.1021/op300326b.
8. Heffels, C., Willemse, A., & Scarlett, B. (1996). Possibilities of near backward light scattering for characterizing dense particle systems. *Powder Technology, 86*(1), 127–135. https://doi.org/10.1016/0032-5910(95)03047-6.
9. Whelan, J., Murphy, E., Pearson, A., Jeffers, P., Kieran, P., McDonnell, S., et al. (2012). Use of focussed beam reflectance measurement (FBRM) for monitoring changes in biomass concentration. *Bioprocess and Biosystems Engineering, 35*(6), 963–975. https://doi.org/10.1007/s00449-012-0681-9.
10. Abu Bakar, M. R., Nagy, Z. K., & Rielly, C. D. (2010). Investigation of the effect of temperature cycling on surface features of sulfathiazole crystals during seeded batch cooling crystallization. *Crystal Growth & Design, 10*(9), 3892–3900. https://doi.org/10.1021/cg1002379.
11. Kail, N., Briesen, H., & Marquardt, W. (2007). Advanced geometrical modeling of focused beam reflectance measurements (FBRM). *Particle & Particle Systems Characterization, 24*(3), 184–192. https://doi.org/10.1002/ppsc.200601036.
12. Tadayyon, A., & Rohani, S. (1998). Determination of particle size distribution by Par-Tec® 100: Modeling and experimental results. *Particle & Particle Systems Characterization, 15*(3), 127–135.
13. Yu, Z. Q., Chow, P. S., & Tan, R. B. H. (2008). Interpretation of focused beam reflectance measurement (FBRM) data via simulated crystallization. *Organic Process Research & Development, 12*(4), 646–654. https://doi.org/10.1021/op800063n.
14. Pandit, A., Katkar, V., Ranade, V., & Bhambure, R. (2019). Real-time monitoring of biopharmaceutical crystallization: Chord length distribution to crystal size distribution for lysozyme, rHu insulin, and vitamin B12. *Industrial and Engineering Chemistry Research, 58*(18), 7607–7619. https://doi.org/10.1021/acs.iecr.8b04613.
15. Zhang, B., Abbas, A., & Romagnoli, J. A. (2011). Multi-resolution fuzzy clustering approach for image-based particle characterization for particle systems. *Chemometrics and Intelligent Laboratory Systems, 107*(1), 155–164. https://doi.org/10.1016/j.chemolab.2011.03.001.
16. El Arnaout, T., & Cullen, P. J. (2017). Non-invasive 3D and 360° optical imaging of micro-particles. *Scientific Reports, 7*(1), 6384. https://doi.org/10.1038/s41598-017-06830-8.

17. El Arnaout, T., & Cullen, P. J. (2020). In situ image processing and data binning strategy for particle engineering applications. *Chemical Engineering and Technology*. https://doi.org/10.1002/ceat.201900311.
18. Gao, Z., Rohani, S., Gong, J., & Wang, J. (2017). Recent developments in the crystallization process: toward the pharmaceutical industry. *Engineering, 3*(3), 343–353. https://doi.org/10.1016/J.ENG.2017.03.022.
19. Wei, H., Yang, C., & Yu, Q. (2017). Contour segment grouping for object detection. *Journal of Visual Communication and Image Representation, 48,* 292–309. https://doi.org/10.1016/j.jvcir.2017.07.003.
20. Larsen, P. A., Rawlings, J. B., & Ferrier, N. J. (2007). Model-based object recognition to measure crystal size and shape distributions from in situ video images. *Chemical Engineering Science, 62*(5), 1430–1441. https://doi.org/10.1016/j.ces.2006.11.018.
21. Ahmad, O., Suleiman, D. J., Gherras, N., Presles, B., Févotte, G., & Pinoli, J.-C. (2012). Recognizing overlapped particles during a crystallization process from in situ video images for measuring their size distributions. *Journal of Electronic Imaging, 21*(2), 0211115. https://doi.org/10.1117/1.jei.21.2.021115.
22. Zou, K., Liu, T., Huo, Y., Zhang, F.-K., & Ni, X. (2017). Image analysis for in situ detection of agglomeration for needle-like crystals.
23. Agimelen, O. S., Jawor-Baczynska, A., McGinty, J., Dziewierz, J., Tachtatzis, C., Cleary, A., et al. (2016). Integration of in situ imaging and chord length distribution measurements for estimation of particle size and shape. *Chemical Engineering Science, 144,* 87–100. https://doi.org/10.1016/j.ces.2016.01.007.
24. Sternberg, S. R. (1983). Biomedical image processing. *Computer, 16*(1), 22–34. https://doi.org/10.1109/MC.1983.1654163.
25. Cho, J. W., Choi, Y. S., & Jeong, K. M. (2019). Performance of the eye-safe LRS and color CCD camera under aerosol environments. *Sensing and Imaging, 20*(1), 10. https://doi.org/10.1007/s11220-019-0232-4.
26. Zapata-Pérez, J., Doménech-Asensi, G., Ruiz-Merino, R., Martínez-Álvarez, J. J., Fernández-Berni, J., & Carmona-Galán, R. (2020). Fixed pattern noise analysis for feature descriptors in CMOS APS images. *Sensing and Imaging, 21*(1), 14. https://doi.org/10.1007/s11220-020-0278-3.
27. El Arnaout, T., Kurki, L., Vaarala, T., Ojala, K., Cullen, P. J., & Sullivan, C. (2016). Crystallization monitoring using simultaneous bright field and PlasDIC imaging. *Chemical Engineering Journal, 300,* 64–74. https://doi.org/10.1016/j.cej.2016.04.126.
28. Huo, Y., Liu, T., Yang, Y., Ma, C. Y., Wang, X. Z., & Ni, X. (2020). In situ measurement of 3D crystal size distribution by double-view image analysis with case study on L-glutamic acid crystallization. *Industrial and Engineering Chemistry Research, 59*(10), 4646–4658. https://doi.org/10.1021/acs.iecr.9b05828.
29. Cardona, J., Ferreira, C., McGinty, J., Hamilton, A., Agimelen, O. S., Cleary, A., et al. (2018). Image analysis framework with focus evaluation for in situ characterisation of particle size and shape attributes. *Chemical Engineering Science, 191,* 208–231. https://doi.org/10.1016/j.ces.2018.06.067.
30. Lu, Z., Zhang, L., Jiang, Y., Zhang, C., Zhang, G., & Liu, M. (2019). Crystal morphology monitoring based on in situ image analysis of L-glutamic acid crystallization. In: *Advances in computer science research*.
31. Rashed, M., & Rashed, E. A. (2017). Double-sided sliding-paraboloid (DSSP): A new tool for preprocessing GPR data. *Computers & Geosciences, 102,* 12–21. https://doi.org/10.1016/j.cageo.2017.02.005.
32. Dimov, I. K., Lu, R., Lee, E. P., Seita, J., Sahoo, D., Park, S.-M., et al. (2014). Discriminating cellular heterogeneity using microwell-based RNA cytometry [Article]. *Nature Communications, 5,* 3451. https://doi.org/10.1038/ncomms4451.
33. Ketteler, R., Freeman, J., Stevenson, N., Ferraro, F., Bata, N., Cutler, D. F., et al. (2017). Image-based siRNA screen to identify kinases regulating Weibel–Palade body size control using electroporation [Data Descriptor]. *Scientific Data, 4,* 170022. https://doi.org/10.1038/sdata.2017.22.
34. Poddar, S., Pedersen, M., & Karar, V. (2018). Color image modification with and without hue preservation. *Sensing and Imaging, 19*(1), 35. https://doi.org/10.1007/s11220-018-0219-6.
35. El Arnaout, T., Cullen, P. J., & Sullivan, C. (2016). A novel backlight fiber optical probe and image algorithms for real time size-shape analysis during crystallization. *Chemical Engineering Science, 149,* 42–50. https://doi.org/10.1016/j.ces.2016.04.025.

36. Schindelin, J., Arganda-Carreras, I., Frise, E., Kaynig, V., Longair, M., Pietzsch, T., et al. (2012). Fiji: An open-source platform for biological-image analysis. *Nature Methods, 9*(7), 676–682. https://doi.org/10.1038/nmeth.2019.
37. Danz, R., Vogelgsang, A., Käthner, R., Zeiss, C., & Plant, G. (2004). PlasDIC—A useful modification of the differential interference contrast according to Smith/Nomarski in transmitted light arrangement. *Photonik, 1,* 42–45.
38. Cameron, R. P., Vogl, U., & Trautmann, N. (2020). Interference-contrast optical activity: a new technique for probing the chirality of anisotropic samples and more. *Royal Society Open Science, 7*(5), 192201. https://doi.org/10.1098/rsos.192201.
39. Zhu, H., Chan, F. H. Y., & Lam, F. K. (1999). Image contrast enhancement by constrained local histogram equalization. *Computer Vision and Image Understanding, 73*(2), 281–290. https://doi.org/10.1006/cviu.1998.0723.
40. Sarkar, D., Doan, X.-T., Ying, Z., & Srinivasan, R. (2009). In situ particle size estimation for crystallization processes by multivariate image analysis. *Chemical Engineering Science, 64*(1), 9–19. https://doi.org/10.1016/j.ces.2008.09.007.
41. Yu, W., Liao, L., Bharadwaj, R., & Hancock, B. C. (2017). What is the "typical" particle shape of active pharmaceutical ingredients? *Powder Technology*. https://doi.org/10.1016/j.powtec.2017.02.043.
42. FDA. (2007). *ANDAs: Pharmaceutical solid polymorphism—Chemistry, manufacturing, and controls information (FDA, USA)*. White Oak: Food and Drug Administration.
43. Datta, S., & Grant, D. J. W. (2004). Crystal structures of drugs: advances in determination, prediction and engineering. *Nature Reviews Drug Discovery, 3*(1), 42–57. https://doi.org/10.1038/nrd1280.
44. Upadhyay, P. P., Pudasaini, N., Mishra, M. K., Ramamurty, U., & Rantanen, J. (2018). Early assessment of bulk powder processability as a part of solid form screening. *Chemical Engineering Research and Design*. https://doi.org/10.1016/j.cherd.2018.05.020.
45. Wang, K., Zhuo, L., Li, J., Jia, T., & Zhang, J. (2020). Learning an enhancement convolutional neural network for multi-degraded images. *Sensing and Imaging, 21*(1), 25. https://doi.org/10.1007/s11220-020-00289-0.
46. Wu, Y., Lin, M., & Rohani, S. (2020). Particle characterization with on-line imaging and neural network image analysis. *Chemical Engineering Research and Design*. https://doi.org/10.1016/j.cherd.2020.03.004.
47. Gao, Z. (2019). Non-classical nucleation phenomena study and following process monitoring and optimization in solution crystallization process. Thesis. Western University. https://ir.lib.uwo.ca/etd/6130/.